A Soluble Activin Receptor Type IIB Prevents the Effects of Androgen Deprivation on Body Composition and Bone Health

Alan Koncarevic, Milton Cornwall-Brady, Abigail Pullen, Monique Davies, Dianne Sako, June Liu, Ravindra Kumar, Kathleen Tomkinson, Theresa Baker, Ben Umiker, Travis Monnell, Asya V. Grinberg, Katia Liharska, Kathryn W. Underwood, Jeffrey A. Ucran, Elizabeth Howard, Joseph Barberio, Matthew Spaits, Scott Pearsall, Jasbir Seehra, and Jennifer Lachey

Acceleron Pharma, Inc., Cambridge, Massachusetts 02139

Androgen deprivation, a consequence of hypogonadism, certain cancer treatments, or normal aging in men, leads to loss of muscle mass, increased adiposity, and osteoporosis. In the present study, using a soluble chimeric form of activin receptor type IIB (ActRIIB) we sought to offset the adverse effects of androgen deprivation on muscle, adipose tissue, and bone. Castrated (ORX) or sham-operated (SHAM) mice received either TBS [vehicle-treated (VEH)] or systemic administration of ActRIIB-mFc, a soluble fusion protein comprised of a form of the extracellular domain of ActRIIB fused to a murine IgG2aFc subunit. *In vivo* body composition imaging demonstrated that ActRIIB-mFc treatment results in increased lean tissue mass of 23% in SHAM mice [19.02 $\pm$ 0.42 g (VEH) versus 23.43 $\pm$ 0.35 g (ActRIIB-mFc), $P < 0.00001$] and 26% in ORX mice [15.59 $\pm$ 0.26 g (VEH) versus 19.78 $\pm$ 0.26 g (ActRIIB-mFc), $P < 0.00001$]. Treatment also caused a decrease in adiposity of 30% in SHAM mice [5.03 $\pm$ 0.48 g (VEH) versus 3.53 $\pm$ 0.19 g (ActRIIB-mFc), NS] and 36% in ORX mice [7.12 $\pm$ 0.53 g (VEH) versus 4.57 $\pm$ 0.28 g (ActRIIB-mFc), $P < 0.001$]. These changes were also accompanied by altered serum levels of leptin, adiponectin, and insulin, as well as by prevention of steatosis (fatty liver) in ActRIIB-mFc-treated ORX mice. Finally, ActRIIB-mFc prevented loss of bone mass in ORX mice as assessed by whole body dual x-ray absorptiometry and micro-computed tomography of proximal tibias. The data demonstrate that treatment with ActRIIB-mFc restored muscle mass, adiposity, and bone quality to normal levels in a mouse model of androgen deprivation, thereby alleviating multiple adverse consequences of such therapy. **(*Endocrinology* 151: 4289–4300, 2010)**

Androgens, such as testosterone in men, regulate lean tissue mass, adipose tissue mass, and bone turnover. Low androgen levels result from congenital conditions, such as hypogonadism, but are also a consequence of normal aging in men, where serum testosterone levels have been shown to decline by 10% during each decade after the age of thirty (1, 2). This age-related decline in testosterone has been implicated as a contributing factor in age-related loss of muscle mass, increase in central (abdominal) adiposity, and development of osteoporosis (3). Furthermore, lowering androgen levels is a therapeutic goal of androgen-deprivation therapies used in patients with androgen-dependent cancers, such as prostate, bladder, and mammary cancers. Unfortunately, this life-prolonging treatment is accompanied by the adverse side-effects of androgen deprivation resulting in increased adiposity, loss of muscle mass, and osteoporosis.

Prostate cancer is the most commonly diagnosed noncutaneous cancer in U.S. men, accounting for nearly 200,000 new cases annually (4). Due to the importance of androgens in the growth of prostate cancer cells, androgen deprivation therapy is considered first-line treatment for

ISSN Print 0013-7227 ISSN Online 1945-7170
Printed in U.S.A.

doi: 10.1210/en.2010-0134 Received February 3, 2010. Accepted May 24, 2010.
First Published Online July 23, 2010

Abbreviations: μCT, Micro-computed tomography; ActRIIB, activin receptor type IIB; BMP, bone morphogenetic protein; CV, coefficients of variation; DEXA, dual-energy x-ray absorptiometry; GDF, growth and differentiation factor; NMR, nuclear magnetic resonance; ORX, orchiectomy; VEH, vehicle treated.

advanced (metastatic) prostate cancer and is also used as adjunct therapy for men receiving radiation for high-risk localized (nonmetastatic) disease (5). Androgen deprivation, which consists of irreversible surgical orchiectomy (ORX) or reversible pharmacologic treatment ("medical castration"), improves survival but can lead to a spectrum of effects that negatively impact quality of life. Prominent among these are: 1) fatigue with decreased muscle mass; 2) osteoporosis with increased risk of fracture; and 3) metabolic alterations with increased adiposity and increased risk of insulin resistance, diabetes, and cardiovascular disease (5–7). Compounding the problem, detrimental changes in these end points often occur with aging even before the commencement of androgen deprivation (8). Thus, there is a need for strategies to reduce the severity of such effects and to improve the quality of life for prostate cancer patients treated with androgen deprivation therapy.

Multiple growth and differentiation factor (GDF) family members, including myostatin (GDF-8), signal through activin receptor type IIB (ActRIIB). These factors have been shown to regulate muscle mass and may also be involved in the regulation of bone quality and adipose mass. Previous research in rodents has demonstrated that inhibition of ActRIIB signaling with a chimeric ActRIIB derivative (ActRIIB-mFc), consisting of the extracellular domain of human ActRIIB fused to a murine IgG2a Fc domain, results in greatly increased muscle mass in healthy mice (9, 10) and mice with amyotrophic lateral sclerosis (11). GDF-11 is another member of the TGF-β family that signals through ActRIIB and is of similar structure to GDF-8. Role of GDF-11 has been implicated in regulation of bone formation throughout development, but until recently GDF-8 has only been associated with muscle tissue growth and maintenance. However, a recent study demonstrated that both GDF-11 and GDF-8 are involved in regulation of skeletal development and may have redundant functions (12). Concerning the regulation of adipose mass, myostatin-deficient mice have increased muscle mass, accumulate less fat throughout life than wild-type control animals, and display resistance to diet-induced obesity (13). This effect of myostatin on fat mass is presumably due to increased muscle mass of myostatin-deficient mice.

Castration/orchiectomy (ORX) in mice produces changes in body composition similar to those in men undergoing androgen deprivation therapy, including reduced weight gain, reduced muscle mass, loss of bone with elevated turnover, and increased fat mass (14–16). Therefore, we used an ORX mouse model of androgen deprivation to investigate the effects of ActRIIB-mFc on muscle mass, bone quality, adiposity, and adiposity-related systemic physiological changes, such as circulating concentrations of adipocyte-derived endocrine factors (adipokines) and accumulation of triglycerides in liver tissue. ACE-031 is the human version of ActRIIB-mFc and is currently in Phase I clinical study in human volunteers, where preliminary results demonstrate that the single dose of ACE-031 increased lean body mass and muscle volume.

Materials and Methods

Construction, expression, and purification of ActRIIB-mIgG2aFc (ActRIIB-mFc)

The ActRIIB extracellular domain (Ser^{19}-Thr^{134}) was obtained by PCR amplification. The purified PCR fragment and the pAIDT4 mIgG2a vector were ligated to create the expression construct, and the sequence was confirmed by double-stranded dideoxy sequencing. The pAIDT4-ActRIIB-mIgG2a construct was transiently transfected into HEK293 cells. After 1 wk of growth at 37 C, the conditioned media were harvested with a two-step column chromatography procedure. The purified ActRIIB-mFc (also termed RAP-031) was eluted from the column and then dialyzed into PBS.

Animals and experimental design

Forty male C57/BL6 mice were randomly assigned to either sham-operated (SHAM) or castrated (ORX) experimental groups at 9 wk of age by Taconic Laboratories (Hudson, NY). The ORX and SHAM animals were allowed to recover for 7 d postsurgery at Taconic and then shipped to our site and allowed to acclimate for another 7 d. All procedures were reviewed and approved by Acceleron Pharma, Inc. Animal Care and Use Committee (IACUC), and all animals were housed in conventional cages with free access to food (regular chow) and water. Before any experimental procedures, all of the metal wound clips were removed and the animals were assessed for proper wound healing. The SHAM and ORX animals were then assigned to either a vehicle-treated group (VEH) or ActRIIB-mFc-treated group (ActRIIB-mFc) and received bi-weekly systemic intraperitoneal administration of TBS or ActRIIB-mFc (10 mg/kg) for 71 d. The ActRIIB-mFc concentration (10 mg/kg) and bi-weekly administration regimen were chosen based on in-house dose-response studies demonstrating maximal efficacy observed with the 10 mg/kg dose on lean tissue mass and pharmacokinetic studies performed in mice, respectively.

Body and terminal tissue weights

Body weights were measured twice per week using an electronic scale at the time of intraperitoneal administration of TBS or ActRIIB-mFc. At study termination date, tissues of interest (muscles, fat depots, and tibias) were surgically removed, weighed using an electronic scale, and properly stored for further analysis. At this time, the ORX animals were also examined to confirm complete removal of testes.

DEXA

Whole body bone composition was analyzed *in vivo* by dual-energy x-ray absorptiometry (DEXA) with a Lunar PIXImus densitometer (GE Medical Systems, Fitchburg, WI) using a high-

resolution digital picture (0.18 × 0.18 pixels, resolution of 1.6 line pairs per millimeter) and software version 2.10. The animals were anesthetized using isoflurane and scanned at study d 0 (before administration of ActRIIB-mFc), and then at d 28, 47, and 71 after treatment initiation. The manufacturer reports the image pixel size of 0.035 mm^2 where the total x-ray absorbance threshold for bone per pixel is applied automatically by the software. To evaluate experimental intrameasurement variability, we performed 10 consecutive scans of three different OVX mice and three SHAM mice. The average (mean) coefficients of variation (% CV) for bone mineral density were 1.37 for the OVX mice and 1.31 for the SHAM mice.

Nuclear magnetic resonance (NMR)

Body composition was analyzed at d 0 (before administration of ActRIIB-mFc), and then at d 14, 28, 47, and 71 after treatment initiation using the MiniSpec LF90 NMR Analyzer (Bruker, Woodlands, TX). The manufacturer reports the theoretical limit of detection/precision as ±0.1 g. To evaluate intrameasurement variability, we performed 10 consecutive scans of three different OVX mice and three SHAM mice. The average (mean) coefficients of variation (% CV) for lean tissue mass were 1.24 and 3.53 for the OVX and SHAM mice, respectively. The average (mean) coefficients of variation (% CV) for fat tissue mass were 0.72 and 3.6 for the OVX and SHAM mice, respectively.

Ex vivo assessment of bone structure by micro-computed tomography (μCT)

Cortical morphometry and trabecular structure of the tibia were evaluated after the experiment termination using a vivaCT 75 small-angle-cone-beam μCT imaging system (Scanco Medical AG, Bassersdorf, Switzerland) with resolution of 20.5–156 μm nominal (pixel size). Transverse CT slices (729) of tibia, starting from the distal end of proximal tibia metaphysis, were acquired using 20.5-μm isotropic voxel size (55 kVp, 145 μA, 2048 samples at 1000 projections per 360°, 350 msec integration time). Images were reconstructed, filtered, and a specimen-specific threshold was applied. The tissue density thresholds of detection were obtained through a combination of the manufacturer's presets and visual inspection. These thresholds were kept constant for all of the evaluated specimens. Trabecular structures were quantified using the first 50 slices distal to the growth plate. Cortical bone parameters were evaluated using 50 slices located 400 slices distal to the growth plate. Trabecular morphometric parameters were computed using a direct three-dimensional approach. Bone volume/total volume fraction (BV/TV, %), trabecular thickness (TbTh, μm), trabecular separation (TbSp, μm), and trabecular number (TbN, mm^{-1}) were assessed. Cortical morphometric parameters were also computed using a direct three-dimensional approach. Bone area (BA, mm^2), cortical thickness (C.Th, mm), endosteal perimeter (E.pm, mm), and periosteal perimeter (P.pm, mm) were assessed. To evaluate intrasample variability, we performed 10 consecutive scans of three different bone samples from OVX mice treated with TBS, OVX mice treated with ActRIIB-mFc, and SHAM mice treated with ActRIIB. The average (mean) coefficients of variation (% CV) for the trabecular bone parameters were as follows for OVX+TBS, OVX+ActRIIB-mFc, and SHAM+ActRIIB-mFc groups: 1.37, 0.98, and 1.73 for bone volume fraction; 1.47, 0.64, and 2.17 for trabecular number; 0.75, 0.98, and 0.88 for trabecular thickness; 1.96, 0.96, and 2.67 for trabecular separation, respectively. The average (mean) coefficients of variation (% CV) for the cortical bone parameters were all less than 1%.

In vivo assessment of abdominal adipose tissue content by μCT

Abdominal adiposity was evaluated in anesthetized animals by using the μCT system described above. Approximately 450–500 transverse CT slices starting from T13 thoracic vertebrae and ending at L5 lumbar vertebrae were acquired by using 41-μm isotropic voxel size (45 kVp, 177 μA, 1024 samples at 1000 projections per 360°, 350 ms integration time). Images were reconstructed, filtered, and a threshold segmenting adipose from other tissue was applied. The tissue density thresholds of detection were obtained through a combination of the manufacturer's presets and visual inspection. These thresholds were kept constant for all of the evaluated specimens. To evaluate intrasample variability, we performed 10 consecutive abdominal scans of three different OVX and SHAM mice treated with TBS. The average (mean) coefficients of variation (% CV) for OVX and SHAM groups were as follows: 2.2 and 1.5 for visceral adiposity, and 1.8 and 4.5 for subcutaneous adiposity, respectively.

In vivo assessment of thigh muscle and adipose tissue content by μCT

Tissue composition of a mid-thigh was evaluated in anesthetized animals by using the micro-computed tomography system described above. Transverse CT slices starting from upper thigh (femoral head) down to middle region of patellar tendon were acquired by using 41-μm isotropic voxel size (45 kVp, 177 μA, 1024 samples at 1000 projections per 360°, 350 msec integration time). Images were reconstructed, filtered, and a threshold segmenting adipose from muscle and other tissue was applied.

Serum analysis

Upon study termination, the animals were euthanized using CO_2 and blood was collected into serum separation tubes. After 10-min centrifugation at 10,000 × g, serum was collected and used for subsequent immunoassays according to manufacturer instructions. Total adiponectin ELISA was purchased from Panomics (Fremont, CA), and the manufacturer reported the minimum detectable limit as 15.6 pg/ml and the assay linear range was 5 μg/ml to 320 μg/ml. The manufacturer also reported intrameasurement and intermeasurement reproducibility with coefficients of variation (% CV) of less than 10% for the mouse assay. Leptin ELISA was purchased from Crystal Chem (Downers Grove, IL). The reported detection range was from 0.2 to 12.8 ng/ml and intraassay as well as interassay % CVs were less than 10%. Insulin ELISA was purchased from Linco Research (St. Charles, MO). The manufacturer reported a linear detection range from 0.2 ng/ml to 10 ng/ml with mean intraassay and interassay % CV of less than 10%. Orchiectomy was confirmed by measuring extracted serum testosterone levels as detected by RIA [Ligand Assay and Analysis Core, University of Virginia Center for Research in Reproduction, supported by Eunice Kennedy Shriver National Institute of Child Health and Human Development/National Institutes of Health Specialized Cooperative Centers Program in Reproduction and Infertility Research (SCCPIR) Grant U54-HD28934]. For the testosterone assay the reportable range was from 14.8 ng/dl to 776.2 ng/dl, and inter-

measurement % CV was less than 10%. For all of the serum assays, the samples reading above the upper limit of detection were diluted and read again.

Histology

Upon study termination, adipose tissue depots and livers were surgically dissected and processed as follows. Adipose tissue depots were fixed overnight in 10% formalin and stored in 70% ethanol. The fixed adipose depots were then paraffin-embedded, sectioned into 10-μm sections, and processed for hematoxylin and eosin stain (H&E). Dissected livers were snap frozen in liquid nitrogen, sectioned into 10-μm sections, and processed for Oil Red O stain. All images of the stained sections were taken using a camera connected to a light microscope.

Data analysis

Comparisons between treatment groups over time (longitudinal) were made using ANOVA followed by LS Means Differences Tukey HSD *post hoc* analysis. Comparisons between groups at a single time point (cross) were made using one-way ANOVA Tukey HSD pair test. Differences were considered statistically significant when the two-tailed P value was ≤ 0.05. All data were analyzed with JMP 8.0 (The SAS Institute, Inc., Cary, NC). Data shown are means ± SEM.

Results

ActRIIB-mFc increases total body mass, total lean tissue mass, and individual muscle mass in SHAM and ORX mice

We investigated effects of ActRIIB-mFc in the orchiectomized (ORX) mouse, an animal model which mimics many of the changes in body composition associated with androgen deprivation therapy. As shown in Fig. 1A, ActRIIB-mFc increased the rate of body mass gain under ORX conditions as well as SHAM conditions relative to treatment with vehicle. By d 71, ORX mice weighed less (28.7 ± 0.75 g) than SHAM mice (30.1 ± 0.64 g, $P < 0.05$), while ActRIIB-mFc increased body weights of both

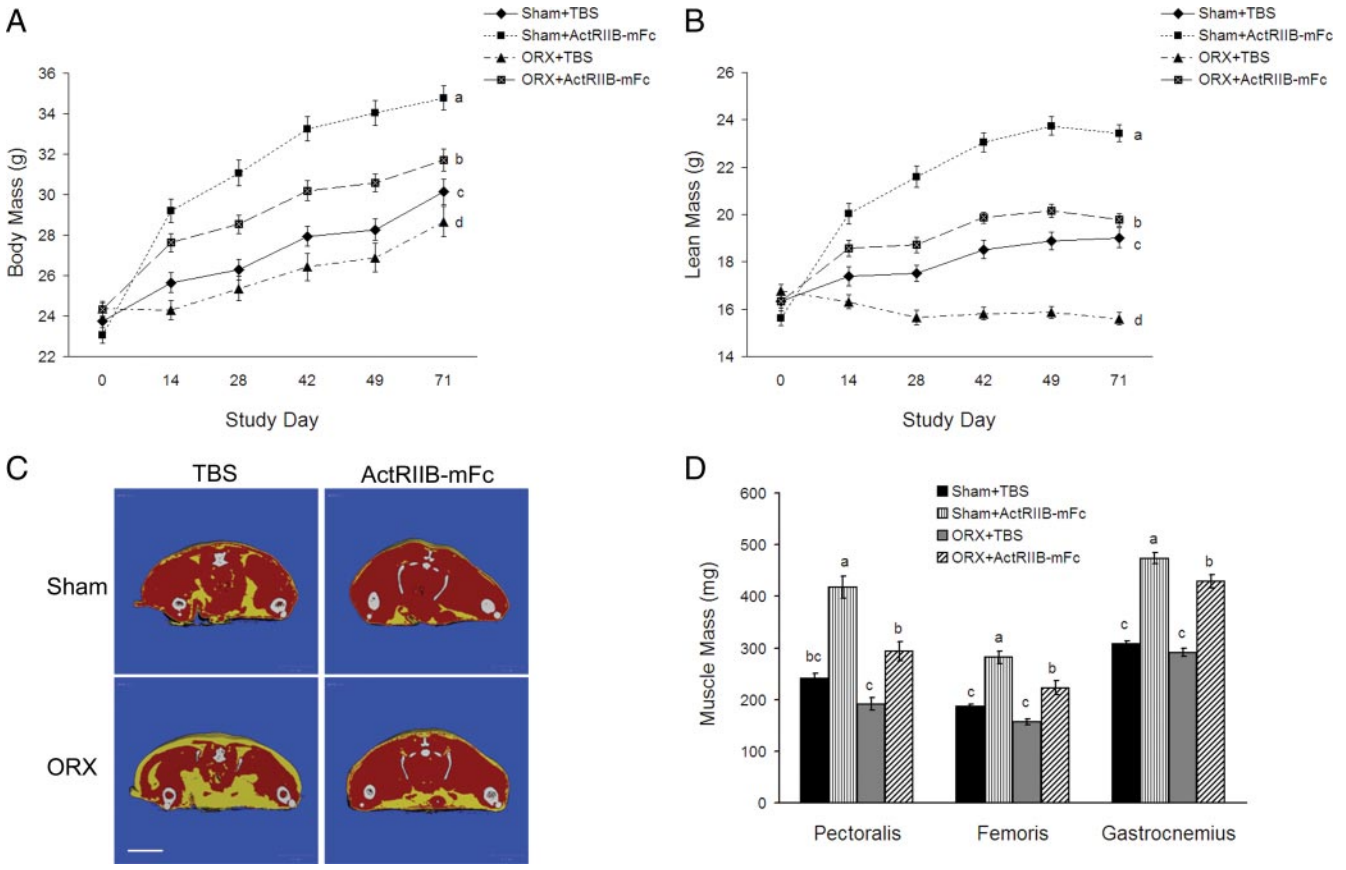

FIG. 1. A, Body weight over time in mice as a function of ORX and ActRIIB-mFc treatment. Vehicle was Tris-buffered saline (TBS). Data shown are means ± SEM (n = 10 per group), and d 71 means that differ significantly ($P < 0.05$) are designated by *different letters* (a, b, c, and d) as determined by ANOVA (longitudinal) and followed by Tukey HSD *post hoc* analysis. B, Lean body mass over time in mice as a function of ORX and ActRIIB-mFc treatment. Vehicle was Tris-buffered saline (TBS). Measurements were made by NMR, data shown are means ± SEM (n = 10 per group), and d 71 means that differ significantly ($P < 0.05$) are designated by *different letters* (a, b, c, and d) as determined by ANOVA (longitudinal) and followed by Tukey HSD *post hoc* analysis. C, Tissue composition in mice as a function of ORX and ActRIIB-mFc treatment for 71 d. Representative micro-CT images of transverse sections at the mid-thigh level indicate muscle (*red*), fat (*yellow*), and bone (*white*). *Scale bar*, 5 mm. D, Muscle mass in mice as a function of ORX and ActRIIB-mFc treatment for 71 d. Pectoralis major, rectus femoris, and gastrocnemius muscles were surgically removed and weighed at study completion. Data shown are means ± SEM (n = 10 per group), and those that differ significantly ($P < 0.05$) are designated by *different letters* (a, b, and c) as determined by one-way ANOVA (cross) Tukey HSD pair test analysis.

TABLE 1. Summary of collected end points at d 71

	SHAM+TBS	SHAM+ActRIIB-mFc	ORX+TBS	ORX+ActRIIB-mFc
Body mass (g)	30.1 ± 0.64^{a}	34.8 ± 0.59^{b}	28.7 ± 0.75^{c}	31.7 ± 0.54^{d}
Lean mass (g)	19.0 ± 0.42^{c}	23.4 ± 0.35^{a}	15.6 ± 0.26^{d}	19.8 ± 0.26^{b}
Lean mass (%)	63.2 ± 1.24^{b}	67.4 ± 0.75^{a}	54.7 ± 1.14^{c}	62.4 ± 0.78^{b}
Fat mass (g)	5.0 ± 0.48^{b}	3.5 ± 0.19^{b}	7.1 ± 0.53^{a}	4.6 ± 0.28^{b}
Fat mass (%)	16.6 ± 1.44^{b}	10.1 ± 0.48^{b}	24.6 ± 1.20^{a}	14.3 ± 0.74^{b}
Serum insulin (ng/ml)	2.20 ± 0.34^{a}	0.77 ± 0.17^{b}	1.20 ± 0.26^{b}	0.79 ± 0.15^{b}
Serum adiponectin (pg/ml)	47.12 ± 1.74^{c}	80.62 ± 4.68^{c}	126.29 ± 5.78^{b}	203.99 ± 19.26^{a}
Serum leptin (ng/ml)	13.38 ± 2.01^{a}	6.38 ± 0.71^{b}	18.56 ± 1.07^{a}	15.16 ± 1.35^{a}
Bone mineral density (g/cm^2)	0.04704 ± 0.00053^{a}	0.04763 ± 0.00054^{a}	0.04503 ± 0.00049^{c}	0.04686 ± 0.00032^{b}
Bone volume fraction	0.2189 ± 0.0231^{c}	0.4864 ± 0.0252^{a}	0.0758 ± 0.0096^{d}	0.3044 ± 0.0190^{b}
Trabecular number (per mm)	3.5598 ± 0.0761^{c}	5.7599 ± 0.1048^{a}	1.9138 ± 0.0952^{d}	4.2188 ± 0.0992^{b}
Trabecular thickness (μm)	0.0860 ± 0.0049^{b,c}	0.1114 ± 0.0054^{a}	0.0714 ± 0.0030^{c}	0.0923 ± 0.0032^{b}
Trabecular separation (μm)	0.2924 ± 0.0078^{b}	0.1462 ± 0.0045^{d}	0.5973 ± 0.0228^{a}	0.2357 ± 0.0070^{c}
Pectoralis major (g)	241.21 ± 9.97^{b,c}	417.54 ± 21.36^{a}	191.27 ± 12.01^{c}	293.34 ± 18.77^{b}
Rectus femoris (g)	186.69 ± 4.20^{c}	281.53 ± 12.68^{a}	156.76 ± 5.71^{c}	222.61 ± 13.30^{b}
Gastrocnemius (g)	307.74 ± 5.91^{c}	473.69 ± 10.61^{a}	291.30 ± 7.77^{c}	428.73 ± 12.39^{b}
Cortical thickness (mm)	0.235 ± 0.005^{b,c}	0.276 ± 0.007^{a}	0.215 ± 0.004^{c}	0.252 ± 0.003^{b}
Cortical density (mg HA/ccm)	1089.0 ± 6.8^{b}	1107.6 ± 6.2^{a}	1066.1 ± 5.7^{c}	1097.4 ± 3.7a^{b}
Endosteal circumference (mm)	2.17 ± 0.05^{a}	2.02 ± 0.04^{a}	2.16 ± 0.05^{a}	2.08 ± 0.05^{a}
Periosteal circumference (mm)	4.09 ± 0.07^{a,b}	4.24 ± 0.04^{a}	3.91 ± 0.07^{b}	4.16 ± 0.05^{a}

Data shown are means ± SEM at d 71 time point.

Levels not connected by the *same letter* (a, b, c, and d) are significantly different.

ORX (31.7 ± 0.54 g, $P < 0.0001$) and SHAM (34.8 ± 0.59 g, $P < 0.0001$) animals (Table 1 and Fig. 1A). This effect was due to a pronounced increase in lean body mass (Fig. 1B). Whereas ORX controls showed a slight decline in lean body mass (15.6 ± 0.26 g) during the course of treatment, ORX mice treated with ActRIIB-mFc displayed a marked increase in lean body mass (19.8 ± 0.26 g), attaining a mean value 25% significantly higher ($P < 0.0001$) than ORX control mice by study completion (Table 1 and Fig. 1B). A similar significant increase in lean body mass was observed under SHAM conditions for ActRIIB-mFc (23.4 ± 0.35 g) compared with vehicle (19.0 ± 0.42 g, $P < 0.0001$). The effects of ORX and ActRIIB-mFc on lean body mass were similar to the above also when lean body mass was expressed as a percentage of the total body mass (Table 1). Representative images of a mid-thigh region obtained by micro-computed tomography (micro-CT) illustrate the similarity of body composition in ORX mice treated with ActRIIB-mFc to that in SHAM controls (Fig. 1C). This increased lean body mass was due to a stimulatory effect of ActRIIB-mFc on muscle mass under both ORX conditions and SHAM conditions. ActRIIB-mFc increased muscle masses of pectoralis major (pectoralis) by 68% ($P < 0.0001$) and 53% ($P < 0.001$), rectus femoris (femoris) by 54% ($P < 0.0001$) and 37% ($P < 0.0001$), and gastrocnemius muscles by 51% ($P < 0.0001$) and 47% ($P < 0.0001$), in both SHAM and ORX mice, respectively (Table 1 and Fig. 1D). ORX mice had smaller pectoralis major (191.27 ± 12.01 g) and biceps femoris muscles (156.76 ± 5.71 g) than SHAM mice (241.21 ± 9.97 g and 186.69 ± 4.20 g, respectively); however, these changes were not significant ($P = 0.087$ and $P = 0.089$, respectively). Gastrocnemius muscle weights did not change as a function of ORX. We also measured serum testosterone levels to confirm orchiectomy and androgen deprivation in ORX mice and, as expected, testosterone concentrations were significantly lower in ORX mice (10.96 ± 0.63 ng/dl) compared with those in SHAM mice (723.98 ± 239.16 ng/dl, $P < 0.001$), with residual amounts in the ORX mice likely due to secretion by the adrenal gland.

ActRIIB-mFc prevents obese phenotype in ORX mice

ActRIIB-mFc also altered fat mass. As determined by NMR, mean total fat mass in ORX controls tripled over the course of the study (Fig. 2A) with the ORX mice ending up with 40% more of total fat (7.1 ± 0.53 g) than the SHAM mice (5.0 ± 0.48 g, $P < 0.001$). ActRIIB-mFc treatment in ORX mice significantly reduced this accumulation by more than 60% ($P < 0.001$) at the end of treatment, effectively maintaining mean fat mass under ORX conditions to levels (4.6 ± 0.28 g) that were not significantly different ($P = 0.1$) from SHAM controls (5.0 ± 0.48 g) at study completion (Table 1 and Fig. 2A). In addition, ActRIIB-mFc reduced the gain in mean fat mass observed in SHAM mice by end of study at d 71, 5.0 ± 0.48 g *vs.* 3.5 ± 0.19 g, respectively; however, this reduction did not reach significance ($P = 0.09$). The effects of both ORX and ActRIIB-mFc were analogous whether expressed as total fat mass or as percentage of the total body mass (Table 1). As shown by micro-CT imaging (Fig. 2B), the abdominal

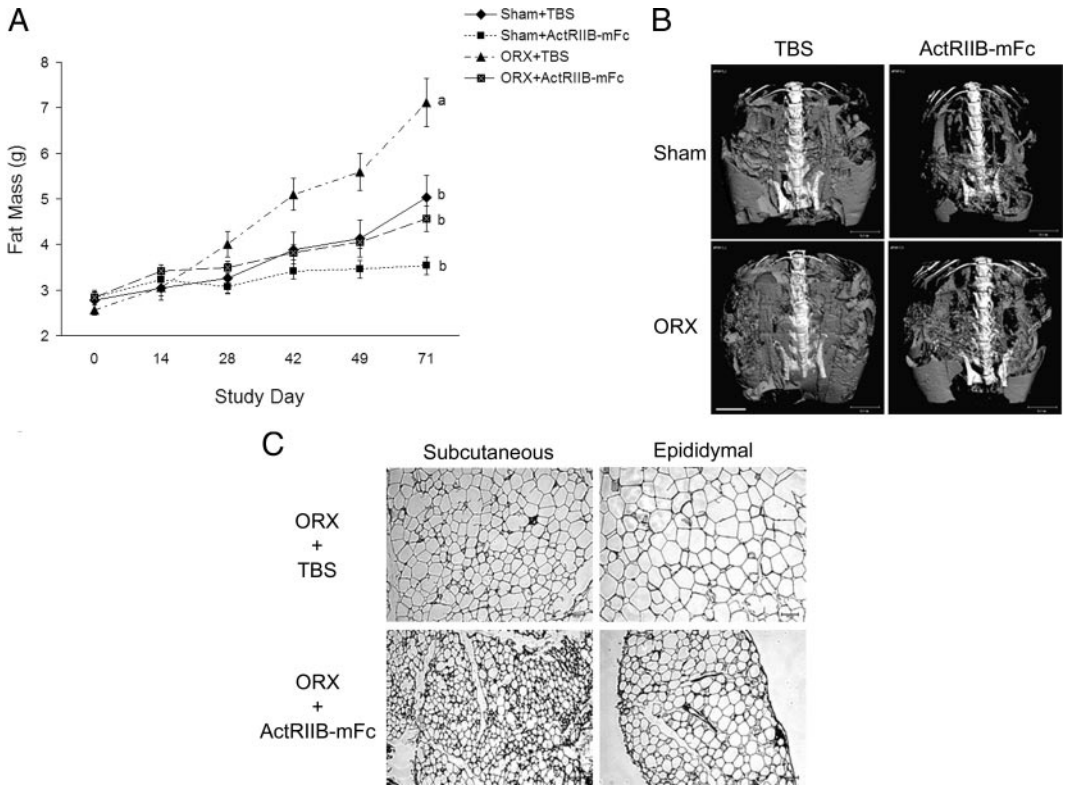

FIG. 2. A, Fat tissue mass over time in mice as a function of ORX and ActRIIB-mFc treatment. Measurements were made by NMR, data shown are means (n = 10 per group), and d 71 means ± SEM that differ significantly ($P < 0.05$) are designated by *different letters* (a and b) as determined by ANOVA (longitudinal) and followed by Tukey HSD *post hoc* analysis. B, Abdominal fat in mice as a function of ORX and ActRIIB-mFc treatment for 71 d. Representative three-dimensional micro-CT images show fat (*gray*) and bone (*white*). *Scale bar*, 5 mm. C, Adipocyte histology in ORX mice treated with vehicle (TBS) or ActRIIB-mFc for 71 d. Sections were stained with hematoxylin and eosin. Magnification, ×10. *Scale bar*, 100 μm.

fat content in ORX mice treated with ActRIIB-mFc was similar to that in SHAM controls. Consistent with these results, a histological analysis of fat depots indicated that ActRIIB-mFc reduced adipocyte size in sc and epididymal depots (Fig. 2C).

ActRIIB-mFc treatment alters circulating adipokine levels and prevents liver steatosis

ActRIIB-mFc treatment significantly reduced mean serum leptin concentrations (Fig. 3A) in SHAM (6.38 ± 0.71 ng/ml, $P < 0.02$), but not ORX (15.16 ± 1.35 ng/ml, $P = 0.36$) mice compared with their vehicle-treated counterparts (13.38 ± 2.01 ng/ml and 18.56 ± 1.07 ng/ml, respectively). Mean leptin concentrations were higher in ORX mice than their SHAM counterparts but did not reach statistical significance ($P = 0.06$). Consistent with previous findings that gonadectomy increases serum adiponectin levels in mice, mean adiponectin concentrations (Fig. 3B) were significantly higher ($P < 0.0001$) under ORX (126.29 ± 5.78 pg/ml) conditions than SHAM conditions (47.12 ± 1.74 pg/ml). ActRIIB-mFc treatment significantly increased mean serum adiponectin concentrations in both ORX (203.99 ± 19.26 pg/ml) and SHAM (80.62 ± 4.68 pg/ml) mice compared with the vehicle-treated groups (126.29 ± 5.78 pg/ml and 47.12 ± 1.74 pg/ml, respectively); however, only the effects in ORX mice reached statistical significance ($P < 0.0001$). The adiponectin concentrations in this study represent the sum of known oligomeric isoforms (total adiponectin). ActRIIB-mFc treatment also significantly reduced mean circulating insulin concentrations (Fig. 3C) under fed conditions compared with SHAM controls (0.77 ± 0.17 ng/ml *vs.* 2.20 ± 0.34 ng/ml, $P < 0.005$) but not ORX controls (0.79 ± 0.15 ng/ml *vs.* 1.2 ± 0.26 ng/ml, $P = 0.07$). Finally, liver triglyceride content visualized by Oil Red O was increased in ORX mice compared with SHAM mice (Fig. 3D), consistent with liver steatosis (*i.e.* fatty liver). This lipid-accumulating effect of ORX was prevented in ORX mice treated with ActRIIB-mFc as seen by fewer Oil Red O stained lipid droplets.

ActRIIB-mFc prevents bone loss in ORX mice

ActRIIB-mFc altered multiple indices of bone quantity and quality. As determined by whole-body analysis with DEXA, ActRIIB-mFc treatment increased bone mineral density under ORX conditions (from 0.04503 ± 0.00049 g/cm^2 to 0.04686 ± 0.00032 g/cm^2, $P < 0.02$) but did not have a significant effect on mean bone mineral density under SHAM conditions (0.04763 ± 0.00054 g/cm^2 *vs.* 0.04704 ± 0.00053 g/cm^2, $P = 0.99$), as determined on d

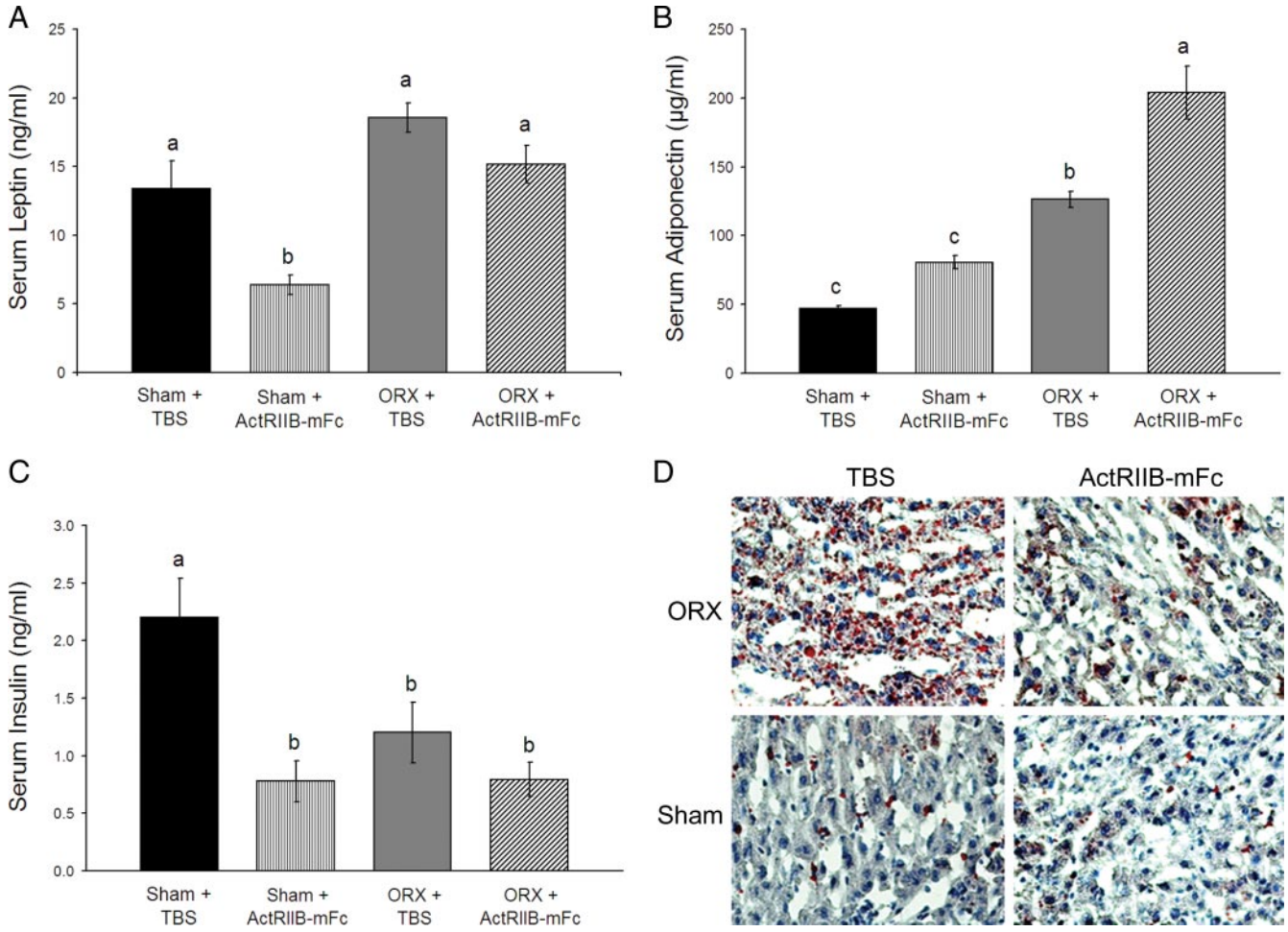

FIG. 3. A, Serum leptin concentrations in mice as a function of ORX and ActRIIB-mFc treatment for 71 d. B, Total serum adiponectin concentrations in mice as a function of ORX and ActRIIB-mFc treatment for 71 d. C, Serum insulin concentrations in mice as a function of ORX and ActRIIB-mFc treatment for 71 d. Data shown are means ± SEM (n = 10 per group), and those that differ significantly ($P < 0.05$) are designated by *different letters* (a, b, and c) as determined by one-way ANOVA (cross) Tukey HSD pair test analysis. D, Liver triglyceride content as a function of ORX and ActRIIB-mFc treatment for 71 d. Liver sections were stained with Oil Red O and visualized using light microscopy. Magnification, ×20.

71 (Fig. 4A). As shown in Fig. 4, B–F, micro-CT analysis of trabecular bone in the proximal tibia at study termination (d 71) revealed that ActRIIB-mFc treatment maintained several bone parameters in ORX mice at levels observed in SHAM controls. With respect to ORX controls, these changes included: 1) a tripling of the mean bone volume fraction from 0.0758 ± 0.0096 to 0.3044 ± 0.0190 ($P < 0.0001$; Fig. 4B), 2) a doubling of mean number of trabeculae per millimeter from 1.9138 ± 0.0952 to 4.2188 ± 0.0992 ($P < 0.0001$; Fig. 4C), 3) increased mean trabecular thickness from 0.0714 ± 0.0030 μm to 0.0923 ± 0.0032 μm ($P < 0.01$; Fig. 4D), and 4) reduced mean trabecular separation from 0.5973 ± 0.0228 μm to 0.2357 ± 0.0070 μm ($P < 0.0001$; Fig. 4E). The similarity of tibial morphology in ORX mice treated with ActRIIB-mFc to that in SHAM controls is evident from representative images shown in Fig. 4F. For each of the foregoing tibia-based end points, ActRIIB-mFc treatment also produced changes in SHAM mice comparable in trend and magnitude to those in ORX mice (Fig. 4, B–F). In addition to improving the trabecular bone parameters, ActRIIB-mFc also improved cortical bone quality of tibias (Fig. 5). ORX mice had significantly lower cortical density (1066.1 ± 5.7 mg HA/ccm *vs.* 1089 ± 6.8 mg HA/ccm, $P < 0.05$), but not thickness (0.215 ± 0.004 mm *vs.* 0.235 ± 0.005 mm, $P = 0.06$), endosteal circumference (2.21 ± 0.05 mm *vs.* 2.22 ± 0.05 mm, $P = 0.10$), and periosteal circumference (3.91 ± 0.07 mm *vs.* 4.09 ± 0.07 mm, $P = 0.18$), than the SHAM controls (Fig. 5). ActRIIB-mFc significantly increased cortical thickness ($P < 0.002$), cortical density ($P < 0.01$), and periosteal circumference ($P < 0.05$) but not endosteal circumference ($P = 0.71$) in ORX mice (Fig. 5, A, B, D, and C, respectively). Endosteal circumference was not significantly different between any two experimental groups, even though it was trending toward lower values as a function of ActRIIB-mFc treatment in both SHAM and ORX mice (Fig. 5C). Changes in the qualitative properties of cortical bones as a function of ORX and

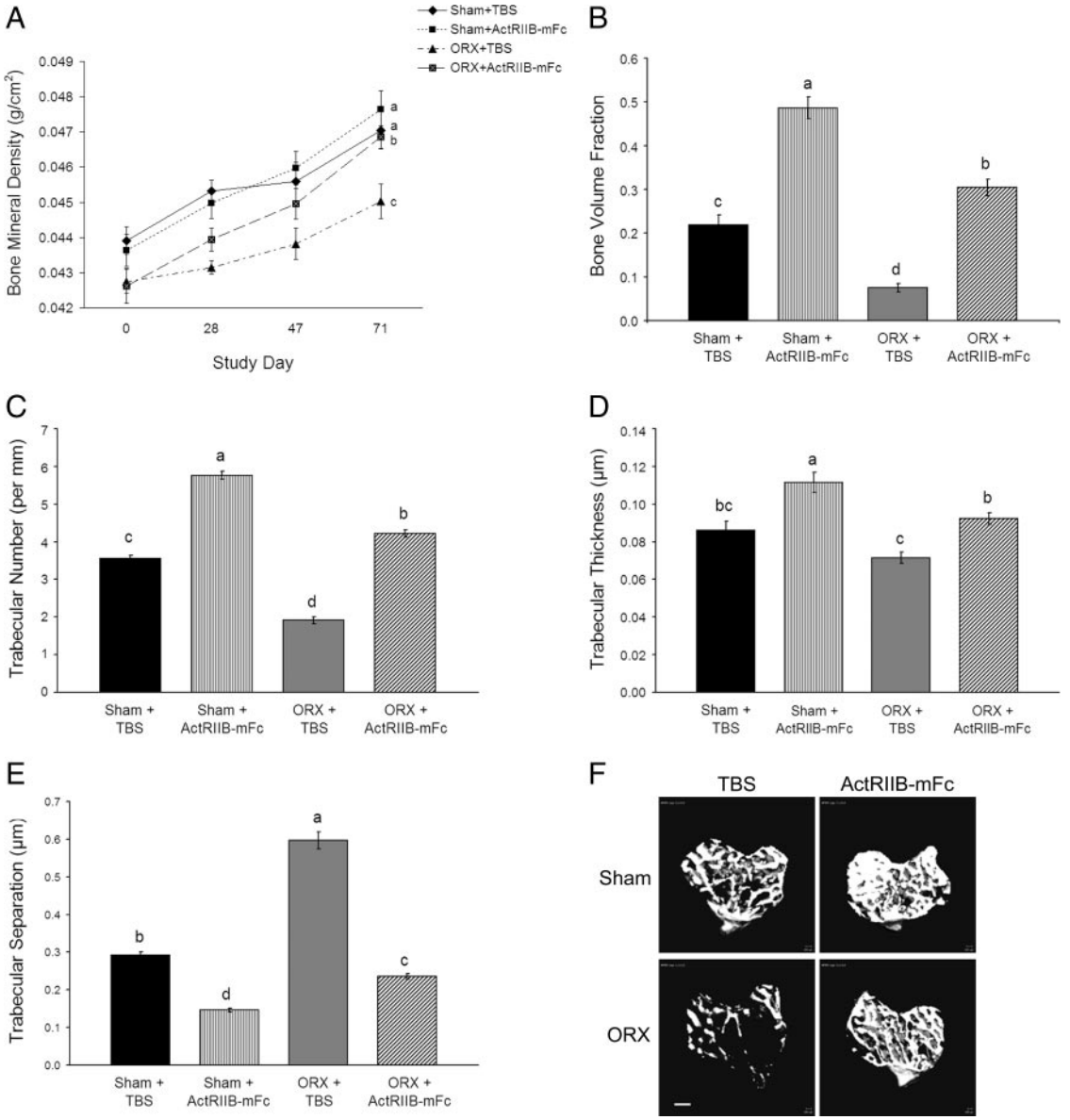

FIG. 4. A, Whole-body bone mineral density over time in mice as a function of ORX and ActRIIB-mFc treatment. Measurements were made by DEXA. Data shown are means ± SEM (n = 10 per group), and d 71 means that differ significantly ($P < 0.05$) are designated by *different letters* (a, b, c, and d) as determined by ANOVA (longitudinal) and followed by Tukey HSD *post hoc* analysis. B, Bone volume fraction in mouse tibia as a function of ORX and ActRIIB-mFc treatment for 71 d. C, Trabecular number in mouse tibia as a function of ORX and ActRIIB-mFc treatment for 71 d. D, Trabecular thickness in mouse tibia as a function of ORX and ActRIIB-mFc treatment for 71 d. E, Trabecular separation in murine tibia as a function of ORX and ActRIIB-mFc treatment for 71 d. For B–E, the measurements were made by micro-CT. Data shown are means ± SEM (n = 7 randomly selected out of the group of 10), and those that differ significantly ($P < 0.05$) are designated by *different letters* (a, b, c, and d) as determined by one-way ANOVA (cross) Tukey HSD pair test analysis. F, Tibial trabecular microarchitecture in mice as a function of ORX and ActRIIB-mFc treatment for 71 d. Shown are representative three-dimensional images of micro-CT-generated transverse sections through trabecular bone in the proximal tibia. *Scale bar*, 350 μm.

ActRIIB-mFc treatment are also evident in the representative μCT images in Fig. 5E.

Discussion

In the current study we investigated the effects of a soluble activin type IIB receptor (ActRIIB-mFc) on multiple adverse effects of androgen deprivation in mice. The only intervention that has been shown to reverse all of the effects of castration is a direct testosterone or dihydroxytestosterone (DHT) supplementation. However, our study demonstrated that ActRIIB-mFc completely prevented muscle mass loss (Fig. 1), fat accumulation (Fig. 2), and bone loss (Figs. 4 and 5) in castrated mice.

The ability of ActRIIB-mFc treatment to overcome the attenuating effects of orchiectomy on body mass, lean mass, and the specific muscles examined (pectoralis, femoris and gastrocnemius) is consistent with its physico-

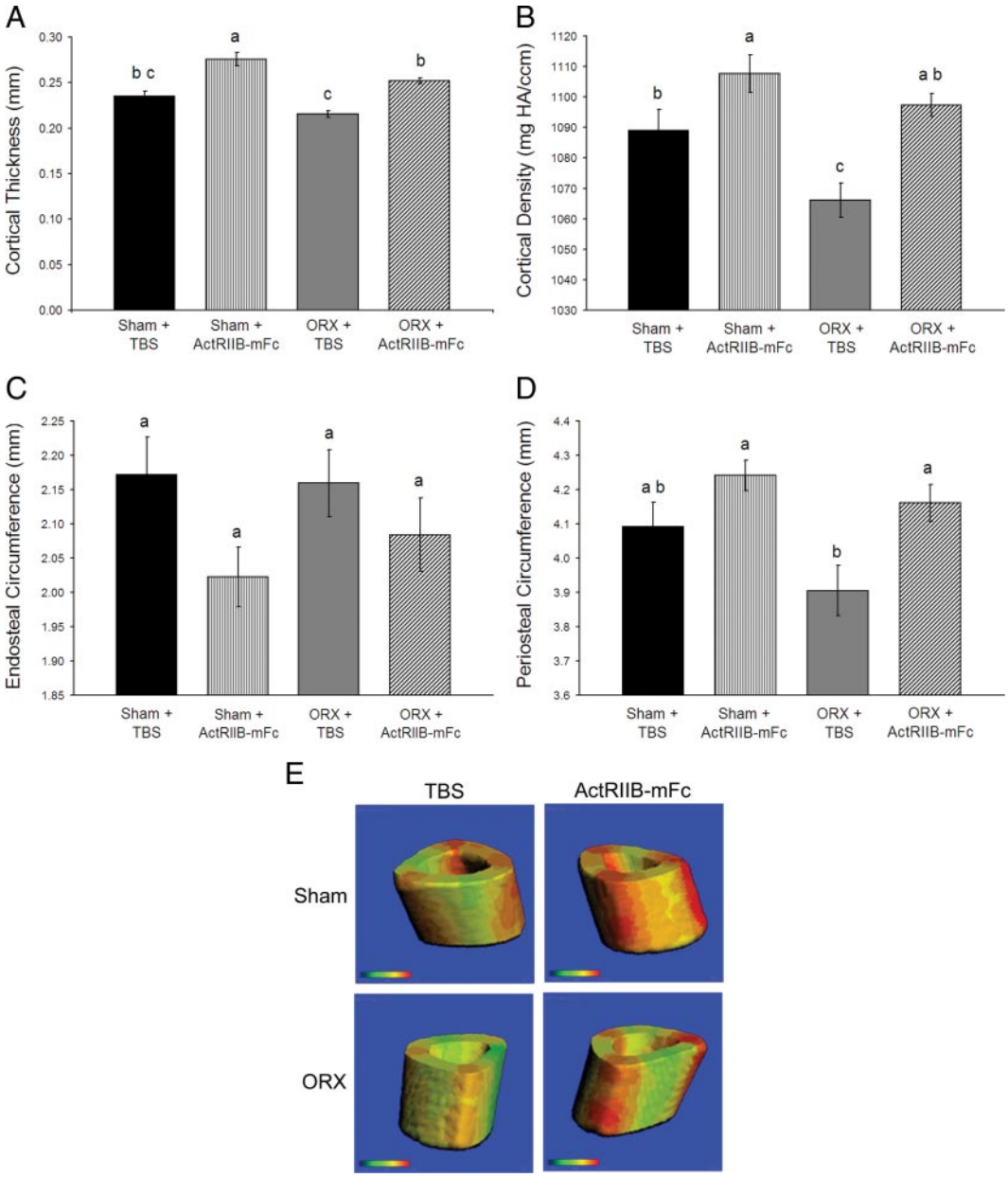

FIG. 5. A, Cortical bone thickness in mouse tibia as a function of ORX and ActRIIB-mFc treatment for 71 d. B, Cortical bone density in mouse tibia as a function of ORX and ActRIIB-mFc treatment for 71 d. C, Endosteal cortical circumference in mouse tibia as a function of ORX and ActRIIB-mFc treatment for 71 d. D, Periosteal cortical circumference in mouse tibia as a function of ORX and ActRIIB-mFc treatment for 71 d. Measurements were made by micro-computed tomography (micro-CT). Data shown are means ± SEM (n = 7 randomly selected out of the group of 10), and d 71 means that differ significantly ($P < 0.05$) are designated by *different letters* (a and b) as determined by one-way ANOVA (cross) Tukey HSD pair test analysis. E, Tibial cortical microarchitecture in mice as a function of ORX and ActRIIB-mFc treatment for 71 d. Shown are representative three-dimensional images of micro-CT-generated cortical bone of the proximal tibias. *Red/brown* areas represent cortical bone of higher density, and *green* areas represent cortical bone of lower density, and *yellow* areas represent bone of intermediate density. *Scale bar*, 100 μm.

chemical properties. This soluble form of the activin type IIB receptor competes with the natural receptor for ligands which include myostatin (GDF-8), a negative regulator of muscle development. Myostatin overexpression results in a decrease in muscle mass in both human (17, 18) and animal (19–21) models, whereas myostatin deficiency results in an enhanced muscular phenotype (22–26). Myostatin signaling occurs via binding with high-affinity to ActRIIB. However, inhibition of ActRIIB signaling produces a greater increase in skeletal muscle than selective inhibition of myostatin alone (9), indicating that ActRIIB mediates both myostatin-dependent and independent regulation of lean tissue mass and could therefore provide a broader-based therapeutic target in the treatment of the muscle-wasting side-effect of androgen depletion strategies such as orchiectomy.

Concerning fat regulation, microarray analysis has shown that adipose tissue expresses activin type I and type

II receptors (27). In addition to inhibiting myogenesis in mesenchymal multipotent cells, GDF-8 also stimulated expression of early and late markers of adipogenesis (28). While GDF-8 has been shown to promote adipogenesis (13, 25), its role in mature adipocyte function is less clear. Mice lacking myostatin gene have less body fat and are resistant to diet-induced obesity (13). Inhibition of myostatin in muscle alone but not fat resulted in decreased fat mass and improved insulin sensitivity (29). Furthermore, a soluble ActRIIB administration reduced body fat in mice fed both regular chow and high-fat diets and resulted in improved insulin sensitivity (30). These current findings suggest that the effects of systemic ActRIIB signaling inhibition on body fat might be predominantly due to the secondary effects of growing muscle tissue on fat storages.

In addition to investigating the effects of ActRIIB-mFc on fat accumulation, we also demonstrated that ActRIIB-mFc promoted a preferred adipokine expression profile accompanied by lower fed insulin levels and prevented liver steatosis in castrated mice (Fig. 3). There is agreement that adiponectin levels generally vary inversely with fat mass and that adiponectin is an insulin-sensitizing adipokine with antidiabetic, antiatherogenic, and cardioprotective properties (31). In the present experiment, adiponectin concentrations were higher under ORX conditions than SHAM conditions, as expected from the known inhibitory effect of testosterone on adiponectin in mice (32). This has been suggested as the reason for obese ORX mice being less likely to develop insulin resistance than diet-induced obese mice. Also, leptin concentrations were higher in ORX mice than their sham counterparts, consistent with increased adiposity and the known inhibitory effect of testosterone on leptin (33).

ActRIIB has been implicated in the binding of a very diverse group of TGF-β family members in addition to myostatin (GDF-8) that regulate bone growth. These include activin A, bone morphogenetic protein (BMP)-7, and BMP-2 (34–37). In the current study we have demonstrated the ability of ActRIIB-mFc treatment to overcome the attenuating effects of orchiectomy on bone quality. It has been suggested that GDF-8 and GDF-11 are derived from one ancestral gene (38). Even though GDF-8 and GDF-11 are highly related members of the TGF-β family of proteins, until recently it was believed that they have very different functions, with GDF-8 being involved only in muscle tissue maintenance and GDF-11 in formation and maintenance of axial skeleton. However, recent findings suggest that GDF-8 and GDF-11 have redundant functions in regulation of skeletal development (12). This study provides evidence for one potential mechanism explaining the effects of ActRIIB-mFc on bone in ORX and SHAM mice seen in our study. Furthermore, activin A is one of the most abundant proteins of the TGF-β/BMP family found in bone, and it has been proposed to be a negative regulator of bone formation. Activin A has a high affinity for both ActRIIA and ActRIIB. It has been demonstrated that treatment with a soluble derivative of ActRIIA leads to increased bone formation, bone mass, and bone strength both in gonad-intact mice and in ovariectomized mice with established bone loss (39). In addition, it was recently reported that soluble ActRIIA-mFc improved bone mass as well as structure in female cynomologus macaques (40) due to both anabolic as well as antiresorptive mechanisms (41). We anticipate that the mechanism of the bone effects reported here with ActRIIB-mFc is due to blocking the same ligand/s as activins as with ActRIIA-mFc (37) and is therefore analogous to the anabolic mechanism responsible for the bone building effects reported with ActRIIA-mFc.

These results demonstrate that treatment with ActRIIB-mFc can alleviate detrimental effects of androgen deprivation on body composition in males. Under androgen-deprived conditions, ActRIIB-mFc reduced adiposity and increased bone quality, lean body mass, and muscle mass. For most end points examined, treatment with ActRIIB-mFc completely prevented detrimental changes associated with androgen deprivation, restoring levels at least to those in SHAM controls. In turn, treatment effects under SHAM conditions were generally comparable in direction and magnitude to those observed under androgen-deprived conditions. Effects of ActRIIB-mFc on body composition were accompanied by significantly elevated concentrations of circulating adiponectin, an important insulin-sensitizing adipokine with antidiabetic, antiatherogenic, and cardioprotective properties. Furthermore, these elevated serum adiponectin levels were correlated with lower insulin levels and lower liver triglyceride content. Taken together, these findings indicate that inhibition of ActRIIB signaling represents a promising adjunct therapeutic paradigm for men receiving androgen deprivation therapy for advanced or high-risk forms of prostate and other types of androgen-dependent cancers. Therefore, it is plausible that the comprehensive improvements in body composition, metabolic parameters, and bone health resulting from ActRIIB-mFc would further increase life quality as well as life expectancy of these patients. The current study investigated preventative effects of ActRIIB signaling inhibition in growing mice that were surgically androgen deprived from young age; therefore, future studies should investigate therapeutic potential of ActRIIB signaling inhibition in adult mice undergoing chemical androgen deprivation therapies, such as androgen antagonist

(bicalutamide and flutamide) or gonadotropin-releasing hormone (GnRH) analog therapies.

Acknowledgments

We thank Tim Ahern for his editorial comments and help with this manuscript. We also thank the manufacturing, bioanalytical, and protein purification groups at Acceleron Pharma, Inc. for their efforts.

Address all correspondence and requests for reprints to: Jennifer Lachey, 128 Sidney Street Cambridge, Cambridge, Massachusetts 02139. E-mail: jlachey@acceleronpharma.com.

Disclosure Summary: All authors are employees of and compensated by Acceleron Pharma, Inc.

References

1. **Travison TG, Araujo AB, Kupelian V, O'Donnell AB, McKinlay JB** 2007 The relative contributions of aging, health, and lifestyle factors to serum testosterone decline in men. J Clin Endocrinol Metab 92: 549–555
2. **Yeap BB** 2009 Testosterone and ill-health in aging men. Nat Clin Pract Endocrinol Metab 5:113–121
3. **Diamond TH** 2005 Pharmacotherapy of osteoporosis in men. Expert Opin Pharmacother 6:45–58
4. **Jemal A, Thun MJ, Ries LA, Howe HL, Weir HK, Center MM, Ward E, Wu XC, Eheman C, Anderson R, Ajani UA, Kohler B, Edwards BK** 2008 Annual report to the nation on the status of cancer, 1975–2005, featuring trends in lung cancer, tobacco use, and tobacco control. J Natl Cancer Inst 100:1672–1694
5. **Sharifi N, Gulley JL, Dahut WL** 2005 Androgen deprivation therapy for prostate cancer. JAMA 294:238–244
6. **Lage MJ, Barber BL, Harrison DJ, Jun S** 2008 The cost of treating skeletal-related events in patients with prostate cancer. Am J Manag Care 14:317–322
7. **Michaelson MD, Cotter SE, Gargollo PC, Zietman AL, Dahl DM, Smith MR** 2008 Management of complications of prostate cancer treatment. CA Cancer J Clin 58:196–213
8. **Daniell HW** 1997 Osteoporosis after orchiectomy for prostate cancer. J Urol 157:439–444
9. **Lee SJ, Reed LA, Davies MV, Girgenrath S, Goad ME, Tomkinson KN, Wright JF, Barker C, Ehrmantraut G, Holmstrom J, Trowell B, Gertz B, Jiang MS, Sebald SM, Matzuk M, Li E, Liang LF, Quattlebaum E, Stotish RL, Wolfman NM** 2005 Regulation of muscle growth by multiple ligands signaling through activin type II receptors. Proc Natl Acad Sci USA 102:18117–18122
10. **Cadena S, Tomkinson KN, Monnell T, Spaits MS, Kumar R, Underwood KW, Pearsall RS, Lachey JL** 13 May 2010 Administration of a soluble activin type IIB receptor promotes skeletal muscle growth independent of fiber type. J Appl Physiol 10.1152/japplphysiol.00866.2009
11. **Morrison BM, Lachey JL, Warsing LC, Ting BL, Pullen AE, Underwood KW, Kumar R, Sako D, Grinberg A, Wong V, Colantuoni E, Seehra JS, Wagner KR** 2009 A soluble activin type IIB receptor improves function in a mouse model of amyotrophic lateral sclerosis. Exp Neurol 217:258–268
12. **McPherron AC, Huynh TV, Lee SJ** 2009 Redundancy of myostatin and growth/differentiation factor 11 function. BMC Dev Biol 9:24
13. **McPherron AC, Lee SJ** 2002 Suppression of body fat accumulation in myostatin-deficient mice. J Clin Invest 109:595–601
14. **Axell AM, MacLean HE, Plant DR, Harcourt LJ, Davis JA, Jimenez M, Handelsman DJ, Lynch GS, Zajac JD** 2006 Continuous testosterone administration prevents skeletal muscle atrophy and enhances resistance to fatigue in orchidectomized male mice. Am J Physiol Endocrinol Metab 291:E506–E516
15. **Hastings IM, Hill WG** 1997 The effect of testosterone in mice divergently selected on fat content or body weight. Genet Res 70:135–141
16. **Vanderschueren D, Vandenput L, Boonen S, Lindberg MK, Bouillon R, Ohlsson C** 2004 Androgens and bone. Endocr Rev 25:389–425
17. **Gonzalez-Cadavid NF, Taylor WE, Yarasheski K, Sinha-Hikim I, Ma K, Ezzat S, Shen R, Lalani R, Asa S, Mamita M, Nair G, Arver S, Bhasin S** 1998 Organization of the human myostatin gene and expression in healthy men and HIV-infected men with muscle wasting. Proc Natl Acad Sci USA 95:14938–14943
18. **Yarasheski KE, Bhasin S, Sinha-Hikim I, Pak-Loduca J, Gonzalez-Cadavid NF** 2002 Serum myostatin-immunoreactive protein is increased in 60–92 year old women and men with muscle wasting. J Nutr Health Aging 6:343–348
19. **Durieux AC, Amirouche A, Banzet S, Koulmann N, Bonnefoy R, Pasdeloup M, Mouret C, Bigard X, Peinnequin A, Freyssenet D** 2007 Ectopic expression of myostatin induces atrophy of adult skeletal muscle by decreasing muscle gene expression. Endocrinology 148:3140–3147
20. **Reisz-Porszasz S, Bhasin S, Artaza JN, Shen R, Sinha-Hikim I, Hogue A, Fielder TJ, Gonzalez-Cadavid NF** 2003 Lower skeletal muscle mass in male transgenic mice with muscle-specific overexpression of myostatin. Am J Physiol Endocrinol Metab 285:E876–E888
21. **Zimmers TA, Davies MV, Koniaris LG, Haynes P, Esquela AF, Tomkinson KN, McPherron AC, Wolfman NM, Lee SJ** 2002 Induction of cachexia in mice by systemically administered myostatin. Science 296:1486–1488
22. **Bogdanovich S, Krag TO, Barton ER, Morris LD, Whittemore LA, Ahima RS, Khurana TS** 2002 Functional improvement of dystrophic muscle by myostatin blockade. Nature 420:418–421
23. **Bogdanovich S, McNally EM, Khurana TS** 2008 Myostatin blockade improves function but not histopathology in a murine model of limb-girdle muscular dystrophy 2C. Muscle Nerve 37:308–316
24. **McPherron AC, Lee SJ** 1997 Double muscling in cattle due to mutations in the myostatin gene. Proc Natl Acad Sci USA 94:12457–12461
25. **McPherron AC, Lawler AM, Lee SJ** 1997 Regulation of skeletal muscle mass in mice by a new TGF-β superfamily member. Nature 387:83–90
26. **Mosher DS, Quignon P, Bustamante CD, Sutter NB, Mellersh CS, Parker HG, Ostrander EA** 2007 A mutation in the myostatin gene increases muscle mass and enhances racing performance in heterozygote dogs. PLoS Genet 3:e79
27. **Carlsson LM, Jacobson P, Walley A, Froguel P, Sjöström L, Svensson PA, Sjöholm K** 2009 ALK7 expression is specific for adipose tissue, reduced in obesity and correlates to factors implicated in metabolic disease. Biochem Biophys Res Commun 382:309–314
28. **Artaza JN, Bhasin S, Magee TR, Reisz-Porszasz S, Shen R, Groome NP, Meerasahib MF, Gonzalez-Cadavid NF** 2005 Myostatin inhibits myogenesis and promotes adipogenesis in C3H 10T(1/2) mesenchymal multipotent cells. Endocrinology 146:3547–3557
29. **Guo T, Jou W, Chanturiya T, Portas J, Gavrilova O, McPherron AC** 2009 Myostatin inhibition in muscle, but not adipose tissue, decreases fat mass and improves insulin sensitivity. PLoS One 4:e4937
30. **Akpan I, Goncalves MD, Dhir R, Yin X, Pistilli EE, Bogdanovich S, Khurana TS, Ucran J, Lachey J, Ahima RS** 2009 The effects of a soluble activin type IIB receptor on obesity and insulin sensitivity. Int J Obes (Lond) 33:1265–1273
31. **Wang ZV, Scherer PE** 2008 Adiponectin, cardiovascular function, and hypertension. Hypertension 51:8–14
32. **Nishizawa H, Shimomura I, Kishida K, Maeda N, Kuriyama H, Nagaretani H, Matsuda M, Kondo H, Furuyama N, Kihara S, Nakamura T, Tochino Y, Funahashi T, Matsuzawa Y** 2002 An-

drogens decrease plasma adiponectin, an insulin-sensitizing adipocyte-derived protein. Diabetes 51:2734–2741
33. **Jockenhövel F, Blum WF, Vogel E, Englaro P, Müller-Wieland D, Reinwein D, Rascher W, Krone W** 1997 Testosterone substitution normalizes elevated serum leptin levels in hypogonadal men. J Clin Endocrinol Metab 82:2510–2513
34. **Hirotani H, Ohtsuka-Isoya M, Mori S, Sakai R, Eto Y, Echigo S, Shinoda H** 2002 Activin A increases the bone mass of grafted bone in C3H/HeJ mice. Calcif Tissue Int 70:330–338
35. **Kawai M, Bessho K, Maruyama H, Miyazaki J, Yamamoto T** 2006 Simultaneous gene transfer of bone morphogenetic protein (BMP) -2 and BMP-7 by in vivo electroporation induces rapid bone formation and BMP-4 expression. BMC Musculoskelet Disord 7:62
36. **Siebenlist S, Kraus T, Burghardt R, Döbele S, Stöckle U, Ganslmeier A** 2010 [Therapy-resistant tibial pseudarthrosis: treatment success with BMP-7 combined with autologous bone.]. Unfallchirurg 113: 59–64
37. **Sako D, Grinberg AV, Liu J, Davies MV, Castonguay R, Maniatis S, Andreucci AJ, Pobre EG, Tomkinson KN, Monnell TE, Ucran JA, Martinez-Hackert E, Pearsall RS, Underwood KW, Seehra J, Kumar R** 12 April 2010 Characterization of the ligand binding functionality of the extracellular domain of activin receptor type IIB. J Biol Chem 10.1074/jbc.M110.114959
38. **Xing F, Tan X, Zhang PJ, Ma J, Zhang Y, Xu P, Xu Y** 2007 Characterization of amphioxus GDF8/11 gene, an archetype of vertebrate MSTN and GDF11. Dev Genes Evol 217:549–554
39. **Pearsall RS, Canalis E, Cornwall-Brady M, Underwood KW, Haigis B, Ucran J, Kumar R, Pobre E, Grinberg A, Werner ED, Glatt V, Stadmeyer L, Smith D, Seehra J, Bouxsein ML** 2008 A soluble activin type IIA receptor induces bone formation and improves skeletal integrity. Proc Natl Acad Sci USA 105:7082–7087
40. **Fajardo RJ, Manoharan RK, Pearsall RS, Davies MV, Marvell T, Monnell TE, Ucran JA, Pearsall AE, Khanzode D, Kumar R, Underwood KW, Roberts B, Seehra J, Bouxsein ML** 2010 Treatment with a soluble receptor for activin improves bone mass and structure in the axial and appendicular skeleton of female cynomolgus macaques (*Macaca fascicularis*). Bone 46:64–71
41. **Lotinun S, Pearsall RS, Davies MV, Marvell TH, Monnell TE, Ucran J, Fajardo RJ, Kumar R, Underwood KW, Seehra J, Bouxsein ML, Baron R** 2010 A soluble activin receptor type IIA fusion protein (ACE-011) increases bone mass via a dual anabolic-antiresorptive effect in cynomolgus monkeys. Bone 46:1082–1088